Highly Improved Mis Photodetector Sensitivity Using Ge Nanocrystals

Mansour Aouassa (mansour.aouassa@yahoo.fr)
Departement of physics, college of arts and sciences, Aljouf University, al qurayyat,
https://orcid.org/0000-0001-5068-9924
Ridha M'gaieth
Université de Monastir: Universite de Monastir
Bilel Azeza
Université de Monastir: Universite de Monastir
Isabelle Berbezier
Aix-Marseille Université III: Aix-Marseille Universite
Luc Favre
Aix-Marseille Université III: Aix-Marseille Universite

Research Article

Keywords: Metal-Insulator-Semiconductor Photodetectors, crystalline Ge nanocrystals, Scanning Electron Microscopy

Posted Date: February 22nd, 2021

DOI: https://doi.org/10.21203/rs.3.rs-217720/v1

Abstract

We report the high performances of Metal-Insulator-Semiconductor Photodetectors (MIS PD) made with crystalline Ge nanocrystals (Ge NCs) as the active absorbers embedded in a silicon dioxide matrix. The Ge NCs have been obtained by a combination of Ge deposition by Molecular Beam Epitaxy (MBE) on tunnel thermal silicon oxide and solid state dewetting processes. Ge NCs structure and morphology are characterized by High Resolution Transmission Electron Microscopy (HRTEM) and Scanning Electron Microscopy (SEM). The photocurrent generation is determined by I-V spectroscopy and Photocurrent spectroscopy. We evidence the role of high quality Ge NCs on photocurrent and explain the high sensitivity of MIS photodetector as a result of transport mechanisms via photoexcited Ge NCs.

These results indicate that the crystalline Ge NCs obtained via solid state dewetting can be integrated with opto-electronics and photonics technologies to produce new high performance optoelectronic devices fully compatible with Complementary Oxide Metal (CMOS) technology.

1. Introduction

At relatively low radiation intensities (i.e. without non-linear effects) the absorption in semiconductors generally follows a Beer-Lambert law which depends on the absorption coefficient of the semiconductor at a given wavelength. [1] To get an active photodetector, i.e. that efficiently absorbs incident radiations in the infrared range and photogenerate charge carriers creating an excess of current in the material, it is essential to choose a semiconductor material that will therefore have a high absorption coefficient in the IR range. In Fig. 1, in the 0,8–1,7μm wavelength range, only three semiconductor materials have a high absorption coefficients including germaniumand III-V ternary (InGaAs) and quaternary (InGaAsP) compounds. [2]

Germanium, after being the basis of the first transistor in 1947, was also used for its photodetection properties from the 1950s in the form of a phototransistor. The first Germanium avalanche photodiodes were developed in the mid-1960s, then during the beginnings of communications by optical fibers where they were in competition with photodiodes based on III-V semiconductors, which were adopted at the expense of Germanium, in particular thanks to their higher performances.[4–5] However since the beginning of the 2000s, technological developments, especially in the field of nanostructures growth, have allowed a renewed interest in Germanium nanostructures, which have become the key nanomaterials for integrated photodetectors on silicon.

The strengths of silicon (and Silicon - Germanium) photonics is the easy integration in conventional microelectronic industry with the use of the same tools, manufacturing processes and base materials. In addition, the devices can be developed on 200 or 300 mm silicon substrates. Such monolithic integration of the devices reduces the number of fabrication steps and consequently the device costs. From this point of view, the use of III-V compound materials is very expensive as compared to the low-cost integration of Ge nanostructures like Ge NCs photodetectors [6]. NCs

Various methods have been developed to create Ge NCs in SiO_2 matrix for optoelectronic devices, including precipitation [7], self-assembly [8], annealing [9], ion implantation [10]. However, Ge NCs based micro-electronic devices prototypes still face some challenges such as anomalous electric transport and low optical absorption and emission.[11] All these problems which cause operating fluctuations and reduce the devices performances, result from fabrication-related defects such as crystalline defects in the Ge NCs, interfacial states at the Ge NCs/SiO_2, NCs size inhomogeneity.

Here we report photocurrent measurements of metal-insulator-semiconductor photodetector (MIS PD) based on high density Ge NCs obtained by deposition using Ultra High Vaccum Solid Source Molecular Beam Epitaxy (UHV-SSMBE) and solid state dewetting. The Ge NCs are then embedded in an insulating layer (SiO_2) during a subsequent step.

During these experiments, the formation of Ge NCs takes place in two steps: first the deposition of amorphous Ge at room temperature on a thin SiO_2 film (and not on the Si substrate). During this step, there is no formation, nor self-organisation of NCs by the Volmer-weber or Stranski Krastanov growth modes (which should involve epitaxial relationships with the substrate and strain relaxation of the crystalline epitaxial layer). At room temperature, the Ge layer remains amorphous. During a second step, the sample is subjected to high temperature annealing. This treatment gives rise to the solid state dewetting phenomenon, based on the Rayleigh-like instability. At sufficiently high temperature, the thin 2D Ge amorphous film crystallizes and reaches a metastable state due to the high energetic cost of the Ge-SiO_2 bonds. The process is accompanied by a rapid diffusion of Ge on SiO_2 which facilitates the dewetting of the Ge crystalline film and promotes the morphological transition from 2D film to 3D islands to reach a lower configurational energy. After dewetting, the surface is fully covered by Ge NCs randomly distributed over the surface. The advantages of this method are first the Ge deposition in an ultra-high vacuum environment preventing any possible contamination and second the control of the Ge NCs size and density with high precision. [12]

2. Experimental

The different fabrication steps are the following: after ex situ chemical cleaning, a 5 nm thin layer of thermal SiO_2 has been grown by rapid thermal oxidation (RTO) process of n-type Si (001) wafers with doping concentration ~ 5 10^{16} cm^3. Then, the substrates have been immediately transferred under clean room atmosphere to the MBE chamber, where the substrates have undergone a thermal cleaning (30 min at 730°C). Then, high purity amorphous Ge thin layers (1 nm and 2 nm) were deposed at room temperature by SSMBE under background pressure of 10^{-11} Torr. The amorphous Ge nanolayers are transformed in-situ into Ge NCs via solid state dewetting during an in-situ annealing step (at 750°C for 30 min) resulting into high density crystalline 3D Ge NCs of well defined shape and randomly distributed on SiO_2 films. After the Ge NCs formation, they are passivated in situ by the deposition of 1 nm amorphous Silicon at room temperature. Such passivation prevents the formation of defects (i.e. GeO_x) at the Ge NCs-SiO_2 top interface that could affect the electrical and optical properties of Ge NCs. [11] All the

samples were then subsequently encapsulated by 45 nm of SiO_2 deposited by Plasma Enhanced Chemical Vapor Deposition (PECVD) during an ex situ step. After the SiO_2 capping, all the samples undergo an ex-situ Rapid Thermal Annealing (RTA) at 750°C for 30s under N_2 ambient gas in order to reduce the defects in the SiO_2 matrix and at the two Ge NCs-SiO_2 interfaces. During a last step, transparent AuPd films (40 nm thick) with surface of 3.2 mm² are deposited by compact plasma sputter coater followed by Rapid Thermal Annealing (RTA) under N_2 at 450°C for 3 min in RTA furnace in order to improve the structural quality of the metal pad and to reduce the interfacial states at the metal-oxide interface. The different fabrication steps are illustrated in Fig. 2:

The distributions in size and density of the Ge NCs were determined from SEM and AFM images. The structural analysis of the Ge NCs was achieved by means of Jeol 2010FX-type High-Resolution Transmission Electron Microscopy (HRTEM).

I-V acquisitions were performed using a Keithley 4200 Source Measure Unit (SMU) interfaced to a computer. A voltage ramp is applied to the sample. The current is measured by the current to voltage converter of the SMU. The maximum resolution of the SMU which does not take into account the parasitic current due to the cables is 10^{-13} A.

The photocurrent spectroscopy is performed using a light beam coming from a tungsten halogen lamp, whose wavelength is varied by passing through the entrance slit of a monochromator (Jobin-Yvon HR640).. Then, the beam obtained at the output of the monochromator is focused on the sample using a lens. The photocurrent is detected as a function of the wavelength and amplified using a current amplifier (Keithley- 428) whose signal is connected to synchronous detection (to improve the signal / noise ratio). The principle of this technique is based on the generation of carriers (electrons and holes) caused by the absorption of photons with energy equal to or greater than the energy gap of the material analyzed. In order to be able to separate and recover the generated carriers (photo-carriers), it is necessary to apply an electric field using contact electrodes. The current is then proportional to the number of incident photons. By varying the wavelength of the photons and taking into account the transfer function of the optical apparatus, we can then determine the absorption spectrum of the material.

3. Results And Discussions

Two MIS photo-detectors with Ge NCs labeled MIS PD_1 and MIS PD_2 are fabricated with small and large Ge NCs respectively. The insertion of crystalline Ge NCs in the insulator of MIS photodetectors structures aims to enhance the photo-response and the electric transport of the MIS photo-detector. The size of the Ge NCs in photodetectors devices was varied to determine its effect on the photo-response and electric transport in MIS photodetectors.

Figure 3 and 4 display both the schematic structure of innovative MIS PD systems and the morphological and structural characterization of the Ge NCs for MIS PD_1 (small NCs) and MIS PD_2 (large NCs) respectively. The SEM image (Figure 3b) of the small Ge NCs obtained from an amorphous Ge layer of 1

nm reveals the formation of high density Ge NCs (5 1011 NCs/cm2) with homogeneous size (mean size around 7nm). Figure 3c and d shows cross sectional HRTEM images of the NCs embedded in the oxide. As already observed in previous studies [7] the Ge NCs are monocrystalline without visible structural extended defects. The mean diameter ~ 7 nm observed by TEM is in good agreement with the SEM observations.

Figure 4b displays the morphology of the large Ge NCs obtained from a deposition of 2 nm amorphous Ge. The density of Ge NCs is reduced as compared to the previous situation (~ 10^{11} NCs/cm^2). Their size distribution is also broader than for a 1nm deposit. As already observed in the past, the Ge NCs size is controlled by the deposited thickness of amorphous Ge (see [7, 12]). Cross section HRTEM images of the Ge NCs (Fig. 4c and d)evidence monocrystalline NCs free of structural defects that have hemispherical shape with high aspect ratios ~ 0.9. The average diameter of these Ge NCs is ~ 14 nm.

From these morphological and structural characterizations we concluded that the Ge NCs are crystalline, with hemispherical shape and homogenous size in the same order of magnitude than the Bohr radius of Ge. Quantum confinement is then expected to occur and should be considered for the interpretation of the results. Since the Ge NCs size can be tailored with high precision by varying the thickness of amorphous Ge initially deposed on the tunnel oxide, the quantized energy could be controlled by varying the thickness of the deposited amorphous Ge layer.

As mentioned above, the Ge NCs are isolated between two insulating barriers: tunnel (t_1 = 5 nm) and capping (t_2 = 45 nm) SiO_2. These two SiO_2 layers are well visible on TEM image (Figs. 3c and 4c). They have been obtained by thermal oxidation (t_1) and by PECVD deposition (t_2) and they exhibit well-known insulating properties. Therefore, the overall conductivity of the Ge NCs / SiO_x matrix system is strongly governed by the properties of the insulator but also by the current through the layer of Ge NCs.

We consider that the conduction current in these structures is continuous and does not depend on the resistance of the system. The latter can be located in the volume of the dielectric or at the interface with the electrodes and corresponds to an extrinsic conduction.

The presence of Ge NCs in insulator affects the transport phenomena in the MIS Photodetector structure. Figure 5a shows the dark current density variation as a function of the applied gate voltage (J-V) for MIS PD_1 (small Ge NCs). The curve is asymmetric with a very large dark accumulation current and a very low dark reverse current as shown at low scale in inset figure in the Fig. 5-a since the transport is governed by the majority carriers which are the electrons because the substrate is N-type doped. To understand the conduction mechanisms in this structure, it is therefore essential to determine all the factors that can affect the electric transport such as the quality and the thickness of the insulating matrix layers. Here, the SiO_2 insulating matrix consist of a capping layer (t_1 = 45 nm) deposited by PECVD and a thermal layer (t_2 = 5nm).

Based on this experimental information, we propose different paths of conduction shown in Fig. 5b to explain the electrical transport mechanisms through the Ge NCs layer. This approach is interesting because it gives information on the effects of structural parameters, considering that the transport of carriers passes mainly through Ge NCs (and not through the traps that may be present in the insulating barriers).

In accumulation regime, at a very low positive gate bias (below 0.3 V), the electrons of the conduction band of the Si substrate cross the tunnel oxide by direct tunnel conduction and afterwards are blocked in the Ge QDs and cannot reach the grid by a direct tunneling process because of the high thickness of the oxide t_2, this is why the current resulting from this mode of conduction denoted (I) is very weak. By increasing the positive gate bias; the barrier of the potential of the oxide seen by the electrons of the substrate becomes triangular, the electrons pass from the conduction band of the substrate to the conduction band of the Ge NCs by direct tunnel conduction then pass from the conduction band of the NCs to the grid by Fowler Nordheim type tunnel conduction through an effective thickness less than that of the oxide. this mode of conduction is denoted (II) in Fig. 5-b. By further increasing the positive gate bias, the potential barrier high of the oxide seen by the electrons decrease further and the conduction mode changes from mode denoted (II) to the mode denoted (III and IV) as shown in Fig. 5b and with each passage, the current increases further.

In inversion regime, at low negative gate bias the electrons in the grid get stuck in front of the thick capping oxide t_2. The carriers therefore cannot reach the Ge NCs by a direct tunnel process and therefore the current cannot go through the Ge NCs. On the other hand, when the barrier seen by the electrons of the grid becomes triangular at high reverse bias, an injection of the Fowler-Nordheim type is possible. This explains the lower dark current density for reverse bias shown in inset Fig. 5a.

Figure 6 shows the comparison of the dark current density variation for MIS PD_1 (small Ge NCs), MIS PD_2 (larger Ge NCs) and MIS structure without Ge NCs (reference structure), We observe that the current density variation of the tow MIS PD has the same shape than the reference sample, but with a significant increase of the current density. This increase in current density is attributed to the intermediate conduction step created by the Ge NCs which significantly increases the crossing probability of the structure. Similar J-V characteristics were reported previously in MIS structures containing Si NCs and attributed this behavior to hopping conduction through the NCs in the barrier [13–15]. The current density increases as a function of NCs size because when the NCs size increases, the percentage of surface covered by the Ge NCs increases. Such phenomenon was observed on all the structures containing Ge NCs studied in this work (not shown here).

In the light of these findings we can conclude that the presence of Ge NCs in the oxide layer of the MIS photodetector increases the current density in MIS structures due to hopping conduction through the Ge NCs.

In addition, we also performed photocurrent measurements on MIS PD devices. The structures are exposed under normal incidence of white light through the large area of transparent metal electrode 3.2 mm^2. When the photons with energy larger than the band gap of the structure illuminate the gate electrode, an electron-hole pair can be generated in Ge NCs or in Si substrate (in the depletion region or in inversion layer) and separated by the built-in electric field. Therefore the generation of electrons in Ge NCs increases and thus the gate current increases. The presence of Ge NCs can then affect the photocurrent generation of electron-holes pairs in the structures as it is explained from the energy band diagram given Fig. 7.

Figure 8 shows the comparison of the current density/voltage (J-V) curves in the dark and under white light illumination for MIS PD with small and large Ge NCs plotted in logarithmic (a-c) and linear (b-d) scales.

For the twos MIS PD devices, there is a strong increase of the forward and reverse photocurrent in presence of Ge NCs under illumination. At forward bias voltage Vg = 1V, the photocurrent density increases from ~ 1 mA/cm^2 to ~ 4 mA/cm^2 for the MIS PD_1 and increase from ~ 2 mA/cm^2 to ~ 7 mA/cm^2 for MIS PD_2.

At reverse bias voltage Vg = 1V, the photocurrent density increases from ~ 4 $\mu A/cm^2$ to ~ 10μ mA/cm^2 for the MIS PD_1 and increase from ~ 5 $\mu A/cm^2$ to ~ 60μ mA/cm^2 for MIS PD_2.

We notice that the reverse photocurrent of MIS PD_2 containing large NCs (14 nm) is 10 times higher than that of MIS PD_1 containing small NCs (7 nm).

The observed evolution is in good agreement with the results reported by Shieh et al. and shows that MIS PD_2 represents a good optimization of the structural and optoelectronic properties. The increase of the photoconductive gain due to the presence of Ge NCs is then explained by the large light absorption and electron-hole pair photo-generation thanks to the presence of high density Ge NCs in the structure. Another mechanism which involves an additional flux of electrons to compensate the positive charges accumulated in the Ge NCs layer (holes are accumulated due to their slower conduction from the substrate through the tunnel oxide) could also explain the results since additional electrons should then travel from the AuPd reservoir (to maintain the charge neutrality) through the control SiO_2 and contribute to the observed photocurrent. A similar gain mechanism was suggested previously for photoconductive gain in GaN/AlGaN metal-semiconductor- metal PDs where holes are trapped by line defects in GaN. [15, 17]

Figure 9 summarizes the evolution of the current density-voltage (J-V) curves in the dark and under white light illumination for MIS reference and MIS PD _ 2 that have a higher photocurrent (in the rest of this work we only focus on this optimized structure). It is clear that the presence of Ge NCs (14 nm) increases strongly the photocurrent signal at low bias indicating that the devices can be operated at a reverse bias as low as 1 V.

To obtain more information about the spectral response we have performed Photocurrent spectroscopy of the optimized structure *MIS PD_2*. In the case of MIS PD, this technique is particularly interesting to explore and determine the absorption threshold (and also indirectly the energy gap) associated with the size of the Ge NCs.

Figure 10 displays the photocurrent spectra obtained on MIS PD_2, only including the excitation wavelength lower than 1000 nm (to eliminate any influence of the silicon substrate on the absorption). These results show a broadband absorption at room temperature associated to Ge NCs in the visible range between 400 nm and 950 nm resulting from high energy confinement in the Ge NCs. And a linear increase of photocurrent measured under 680 *nm low light power density. These results* are very interesting, for improving the spectral response of MIS PD and the realization of high-efficiency PDs that can be easily integrated into a standard silicon complementary metal-oxide semiconductor process. The results also prove that the elaboration method of ultra pure Ge NCs- MIS PD by a combination of MBE deposition and subsequent dewetting is currently the most mature of all published methods.

4. Conclusion

A novel MIS photodetector based on high density ultra-pure crystalline germanium nanocrystals obtained by deposition of amorphous Ge at room temperature in MBE chamber followed by solid state dewetting was demonstrated. We have shown that the Ge NCs inserted in MIS PD enhance the optical sensitivity and the photocurrent generation in MIS photodetector by the large generation of electron-hole pairs and lowering the potential barrier via the holes trapping in the valance band of the Ge NCs. The J-V and photocurrent measurements demonstrate that this novel Ge NCs based MIS photodetector can function in a very wide spectral range and under low reverse bias about 1 V.

Declarations

Due to technical limitations, Declarations Section is not available for this version.

References

1. Hossain, T. -H. Kwon and K. -D. Kim, "Comparison of Different Wavelengths for Estimating SpO2 Using Beer-Lambert Law and Photon Diffusion in PPG," 2019 International Conference on Information and Communication Technology Convergence (ICTC), Jeju Island, Korea (South), 2019, pp. 1377-1379,
2. Giudice, A. Sciuto, A. Meli, G. D'Arrigo and D. Longo, "SO2 Monitoring With Solid State-Based UV Spectroscopy Compact Apparatus," in IEEE Sensors Journal, vol. 19, no. 16, pp. 7089-7094, 15 Aug.15, 2019, doi: 10.1109/JSEN.2019.2913221.
3. O.Kasap, Optoelectronics and Photonics, Principles and Practices, Prentice-Hall International (2001)
4. Fiona E. Thorburn, Laura L. Huddleston, Jarosław Kirdoda, Ross W. Millar, Lourdes Ferre-Llin, Xin Yi, Douglas J. Paul, Gerald S. Buller Proceedings Volume 11386, Advanced Photon Counting Techniques

XIV; 113860N (2020) https://doi.org/10.1117/12.2559620

5. D. Hwanga, Y. E. Hwang, and Y. A. Chen; Appl. Phys. Lett. 117, 091104 (2020); https://doi.org/10.1063/5.0020202
6. Joan Manel Ramírez, Hajar Elfaiki, Théo Vérolet, Claire Besançon, Delphine Néel, Karim Hassan, Christophe Jany, Stéphane Malhouitre, Alexandre Shen, Christophe Caillaud, Dalila Make, Harry Garriah, Jean Decobert, Mohand Achouche, "The hybrid III-V on Si photonic platform revisited: achievements and challenges (Conference Presentation)," Proc. SPIE 11288, Quantum Sensing and Nano Electronics and Photonics XVII, 112881G (10 March 2020);
7. Ordered arrays of Si and Ge nanocrystals via dewetting of pre-patterned thin films Isabelle Berbezier, Mansour Aouassa, A Ronda, Luc Favre, Monica Bollani, Roman Sordan, A Delobbe, P SudraudJournal of Applied Physics 113 (6), 064908
8. M Aouassa, L Favre, A Ronda, H Maaref, I Berbezier Design of free patterns of nanocrystals with ad hoc features via templated dewetting annealing. New Journal of Physics 14 (6), 063038
9. K Das; M. L. N. Goswami; A Dhar; B. K. Mathur and S. K. Ray; Nanotechnology, Volume 18, Number 17. https://doi.org/10.1088/0957-4484/18/17/175301
10. Spind berger, L.; Aber , J.; Polimeni, A.; Schuster, J.; Hörschläger, J.; Truglas, T.; Groiss, H.; Schäffler, F.; Fromherz, T.; Brehm, M. In-Situ Annealing and Hydrogen Irradiation of Defect-Enhanced Germanium Quantum Dot Light Sources on Silicon. Crystals 2020, 10, 351.
11. Bonilla, Isabel Al-Dhahir, Mingzhe Yu, Phillip Hamer, Pietro P. Altermatt, Charge fluctuations at the Si–SiO2 interface and its effect on surface recombination in solar cells, Solar Energy Materials and Solar Cells, Volume 215, 2020,110649.
12. Aouassa, L. Favre, A. Ronda, H. Maaref and I. Berbezier, The kinetics of dewetting ultra-thin Si layers from silicon dioxide. New Journal of Physics, Volume 14, June 2012.
13. B De Salvo, P Luthereau, T Baron, G Ghibaudo, F Martin, D Fraboulet, G Reimbold, J Gautier, Transport process in thin SiO2 films with an embedded 2-D array of Si nanocrystals, Microelectronics Reliability, Volume 40, Issues 4–5, 2000,
14. Stavarache, I., Teodorescu, V.S., Prepelita, P. et al. Ge nanoparticles in SiO2 for near infrared photodetectors with high performance. Sci Rep 9, 10286 (2019).
15. High-efficiency silicon-compatible photodetectors based on Ge quantum dots S. Cosentino, Pei Liu, Son T. Le, S. Lee, D. Paine, A. Zaslavsky, D. Pacifici, S. Mirabella, M. Miritello, I. Crupi, and A. Terrasi.
16. Zhenrui Yu and Mariano Aceves-Mijares; A ultraviolet-visible-near infrared photodetector using nanocrystalline Si superlattice. Appl. Phys. Lett. 95, 081101 (2009);
17. K. Zhang, W. B. Wang, and I. Shtau; Backilluminated GaN/AlGaN heterojunction ultraviolet photodetector with high internal gain. Appl. Phys. Lett. 81, 4862 (2002).

Figures

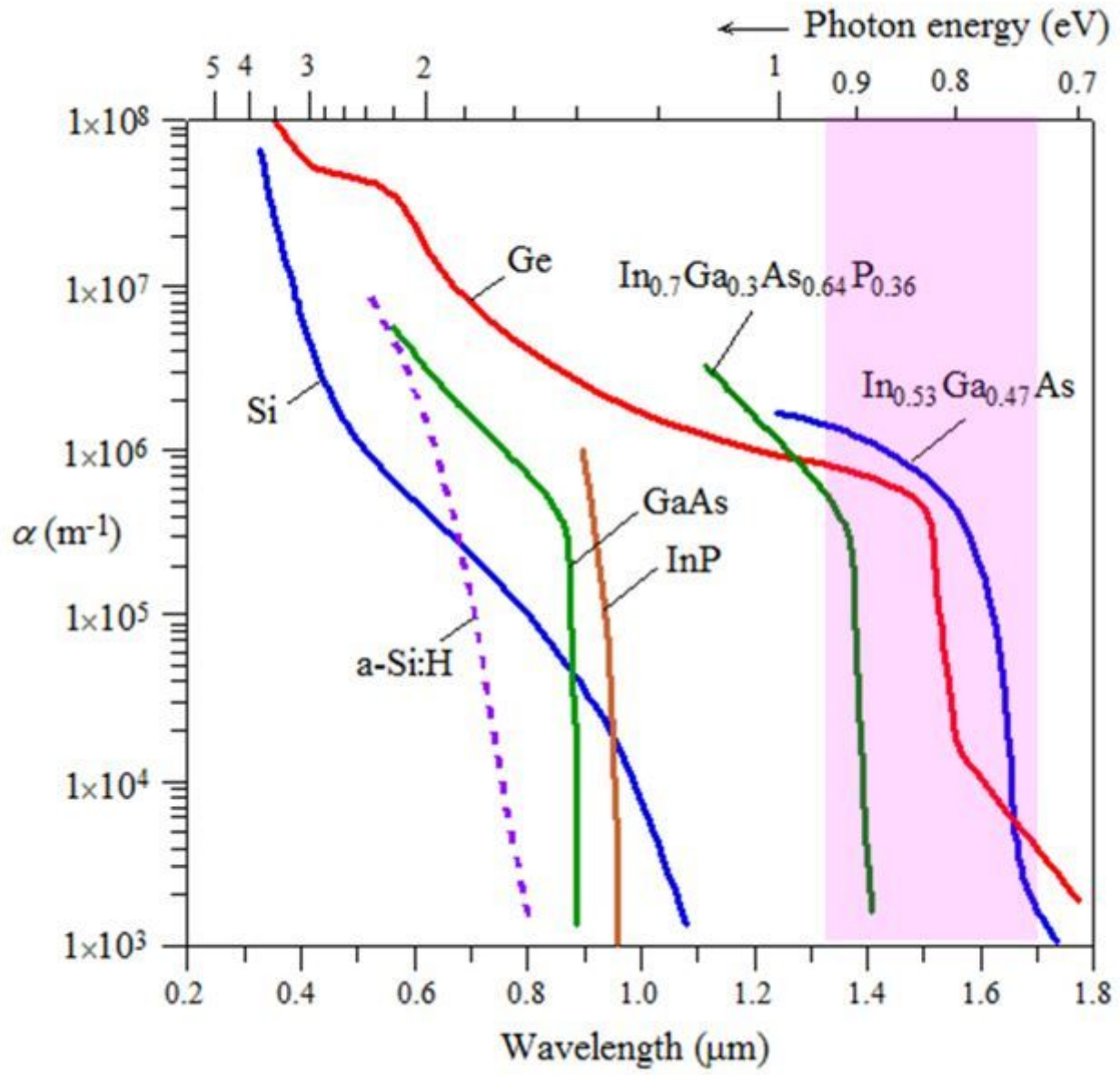

Figure 1

Absorption coefficient as a function of photon wavelength for few typical semiconductors (from [3]).

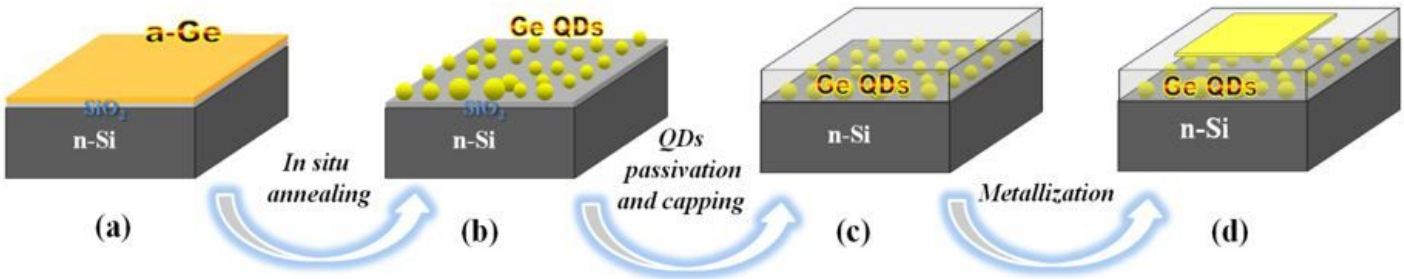

Figure 2

Schematic representation of the fabrication steps of the photodetector: (a) deposition of 2D amorphous Ge nanolayers on SiO2/Si substrate (b); formation of Ge NCs via solid state dewetting (c); Ge NCs surface passivation by capping with amorphous Si (d); Deposition of transparent AuPd electrodes.

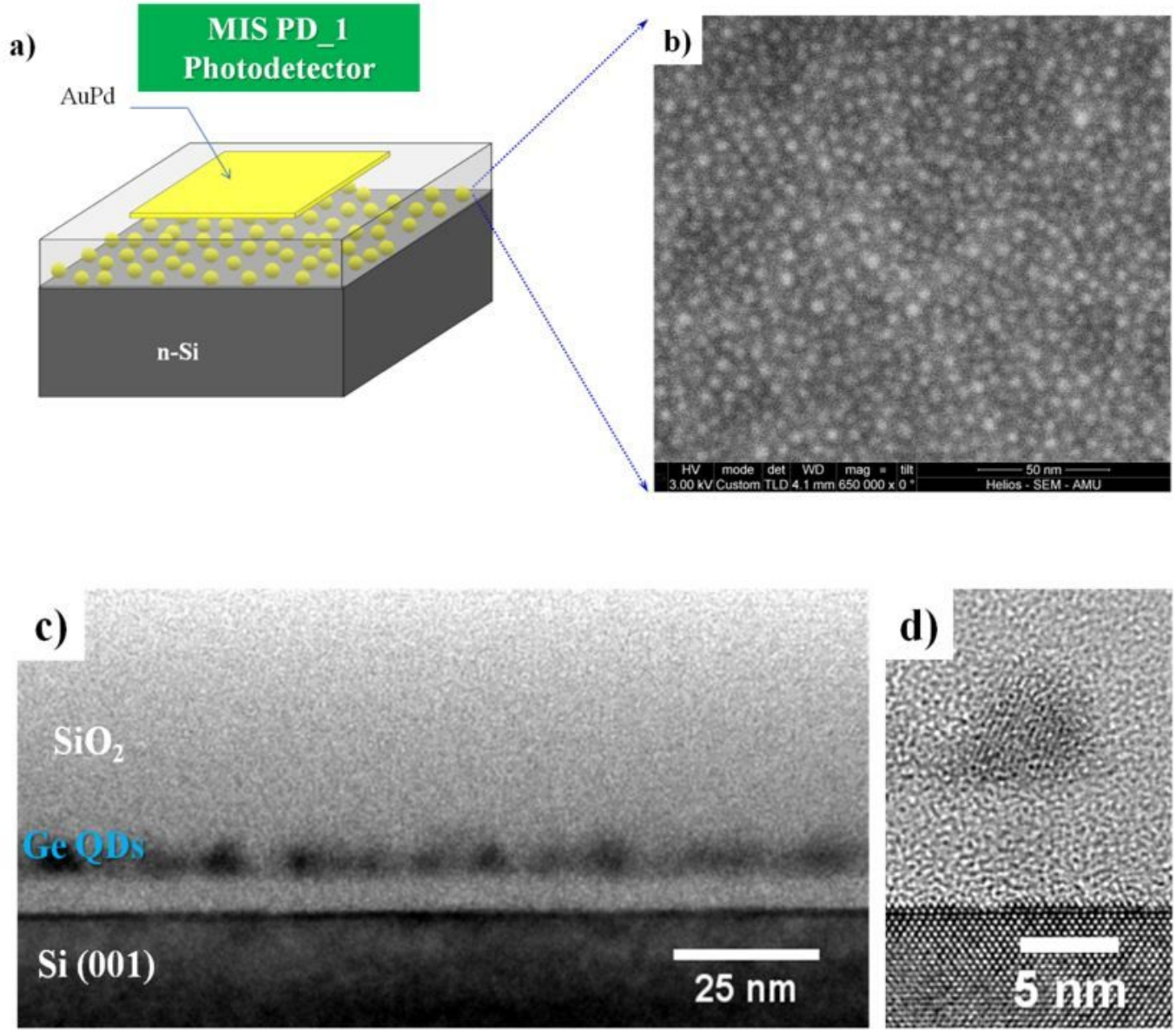

Figure 3

(a) Schematic structure of MIS photodetector with small Ge NCs (d~7 nm); (b) SEM image of the Ge NCs (c and d); Cross-section TEM images of the Si(001) substrate / SiO2 / Ge NCs / SiO2 stacking at low (c) and high (d) magnification.

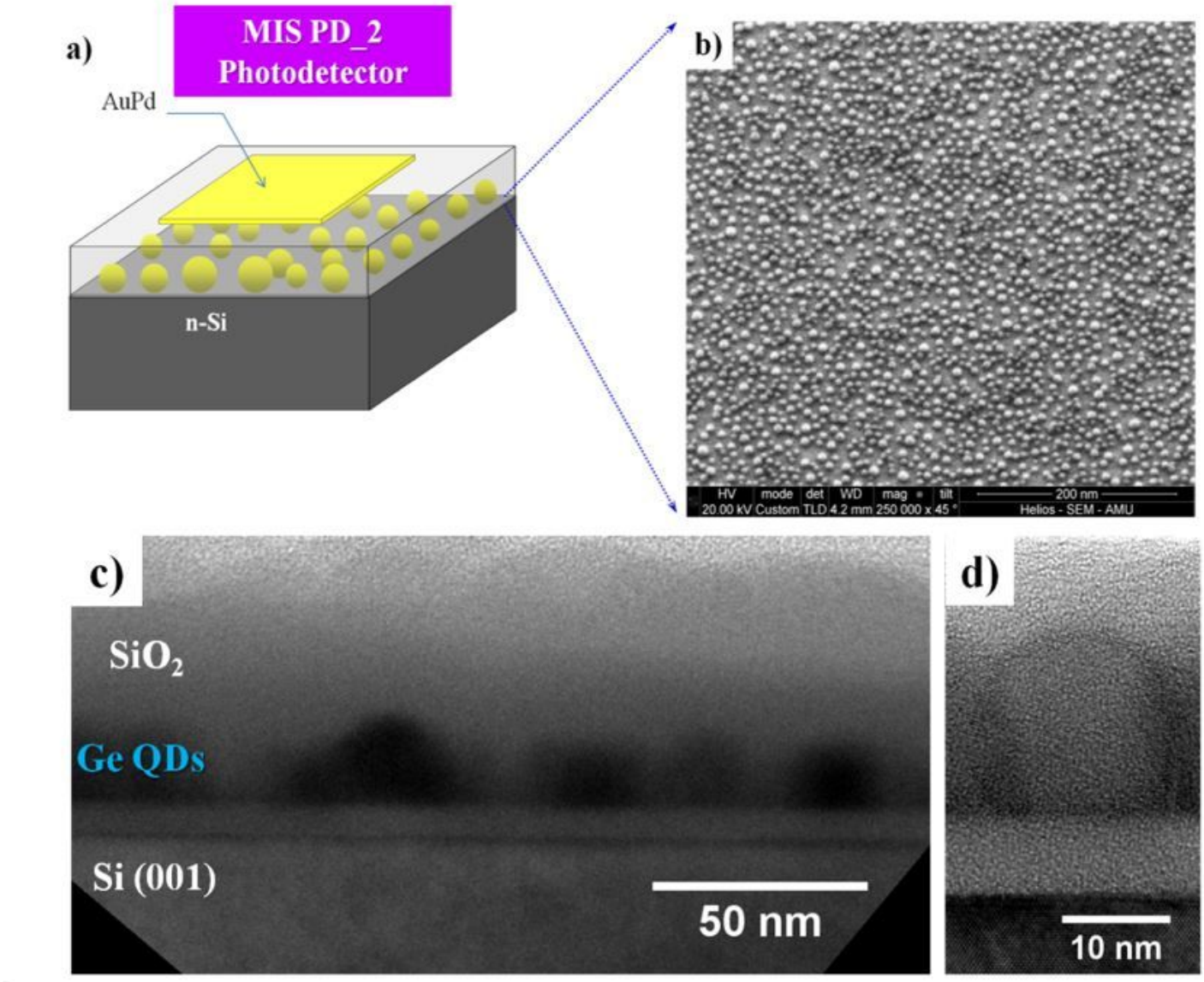

Figure 4

(a) Schematic structure of MIS photodetector with large Ge NCs. (b) SEM image of the Ge NCs (d~14nm). (b and c) TEM image of the device structure at low (b) and high (c) magnification.

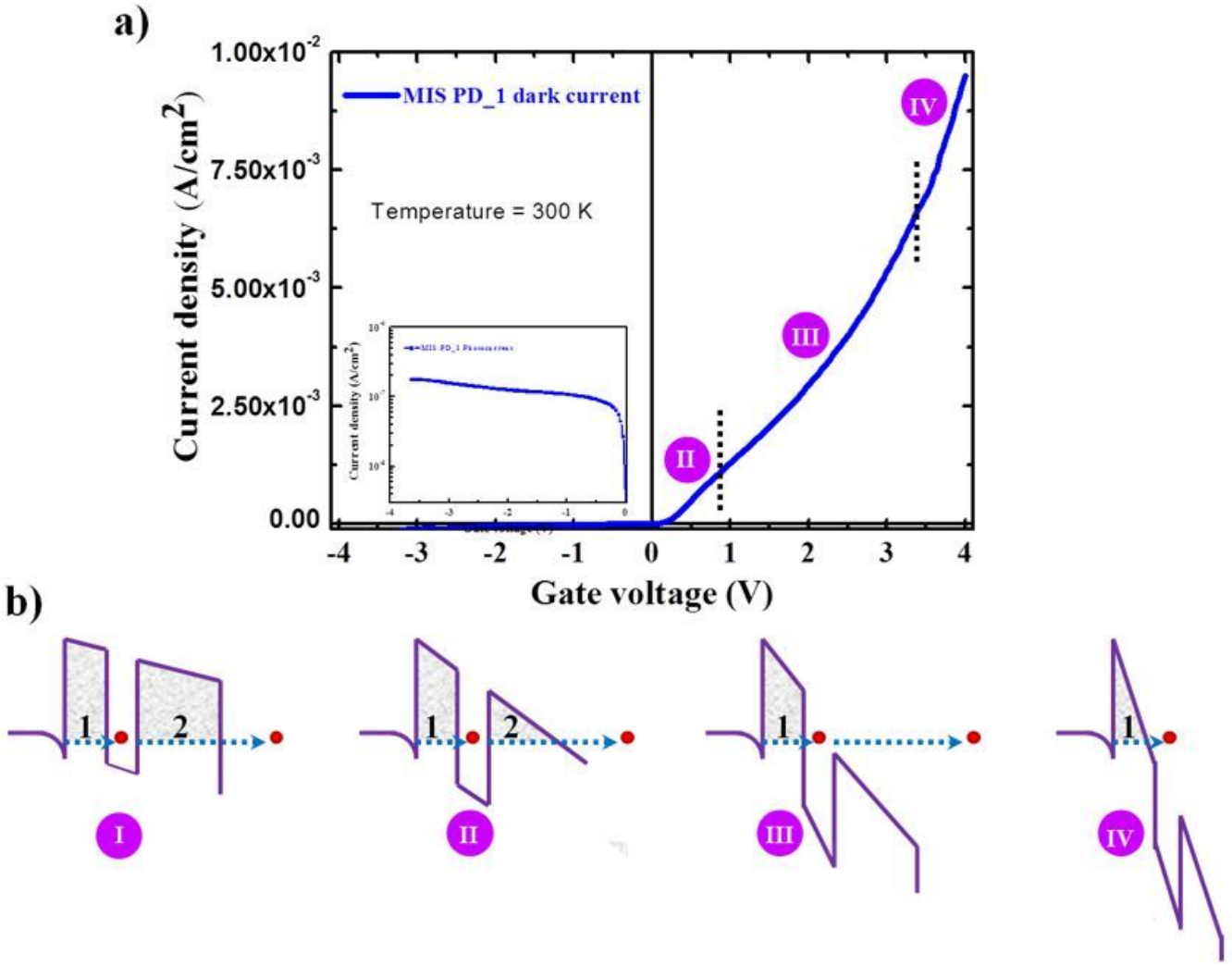

Figure 5

(a). The current density vs. voltage (J–V) characteristic of (MIS PD_1) in darkness. The inset shows zoom in of the reverse dark current density (b). Schema of the band diagrams for different electric fields applied to the MIS PD structures with Ge NCs

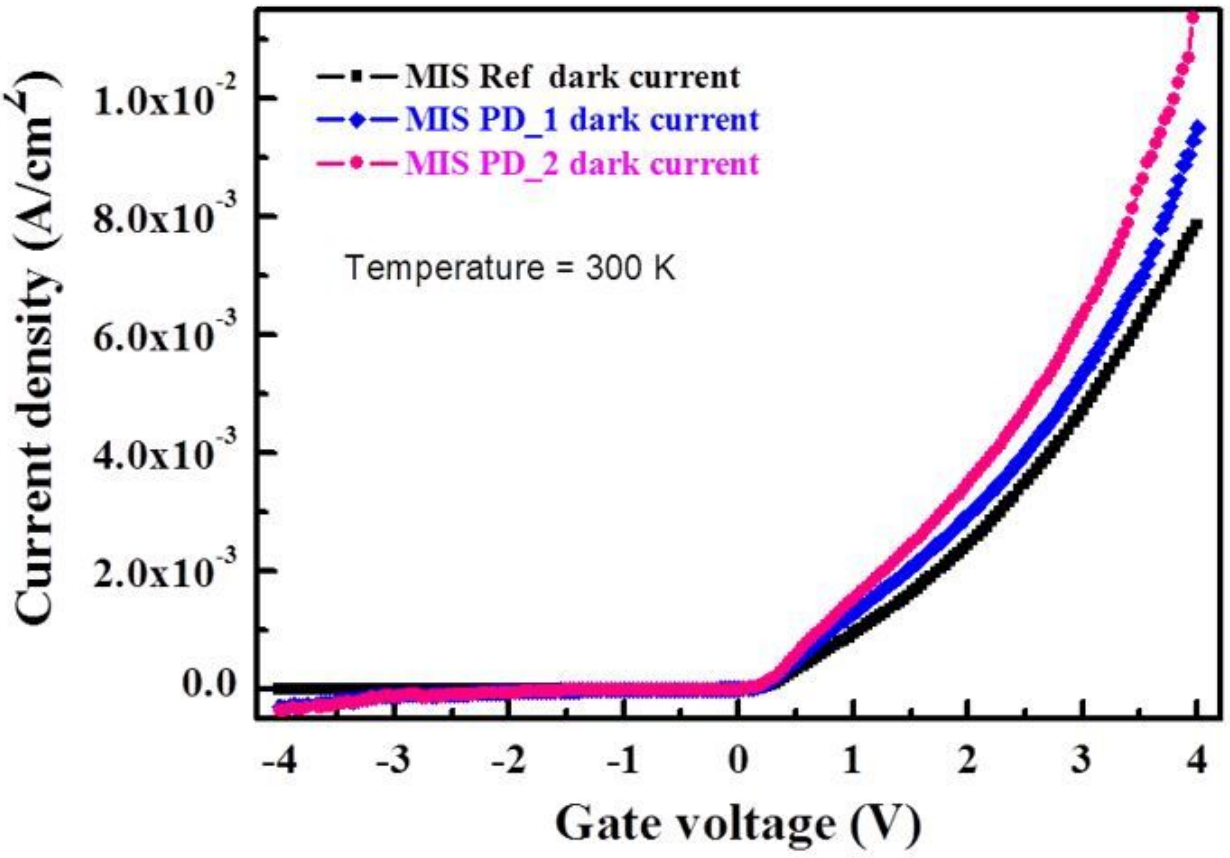

Figure 6

Comparison of the dark current density variation for MIS PD_1 (small Ge NCs), MIS PD_2 (larger Ge NCs) and MIS reference structure (without NCs)

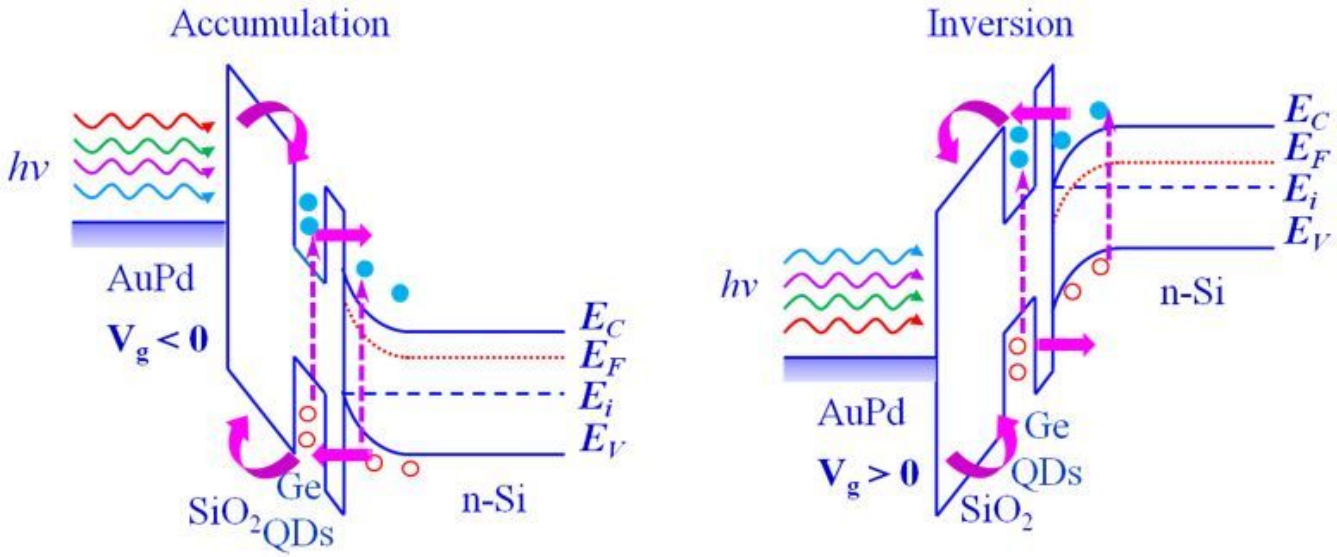

Figure 7

Schematic diagram of photocurrent mechanisms in MIS PD with Ge NCs during (a) inversion and (b) accumulation regimes.

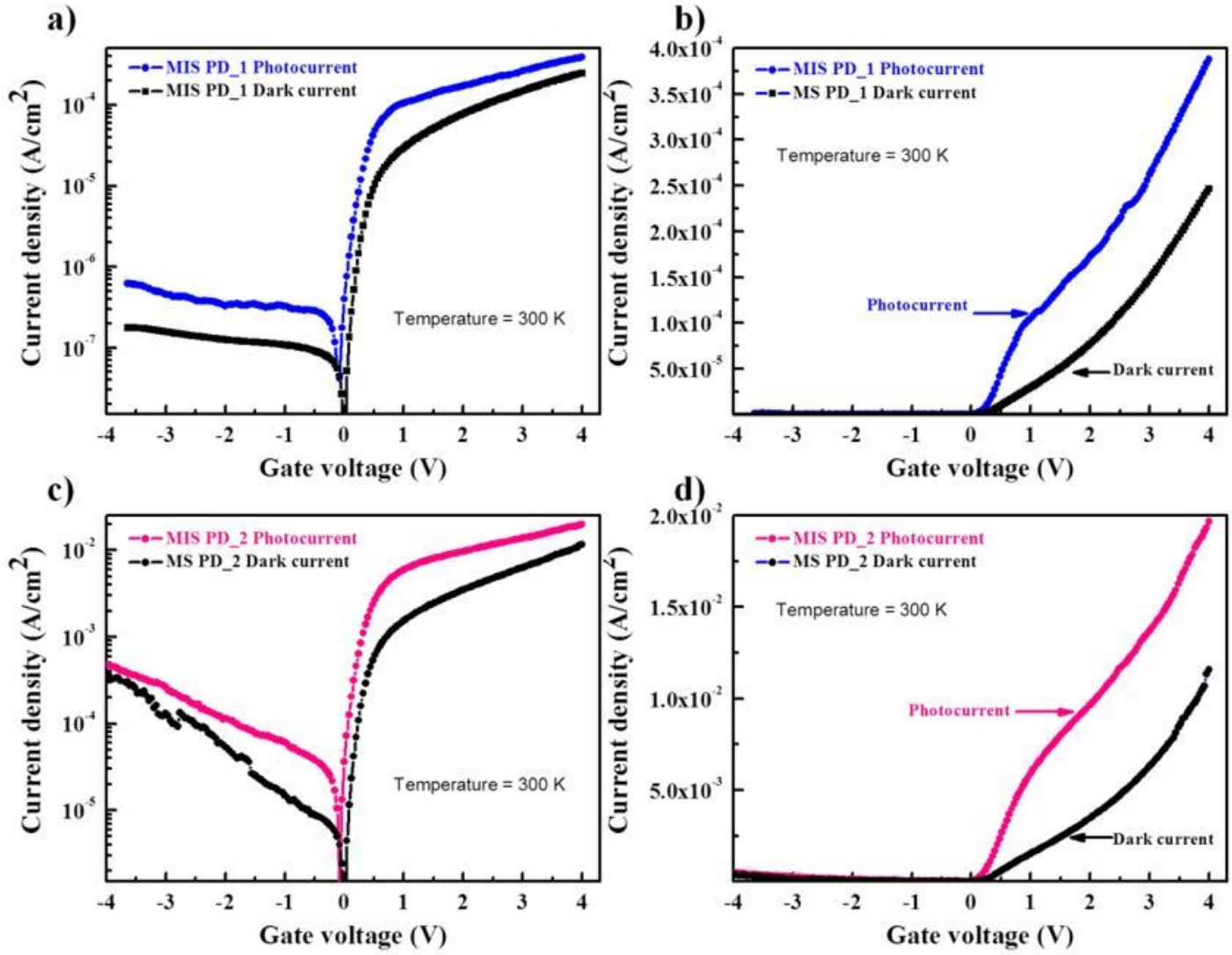

Figure 8

Evolution of the current density - voltage (J-V) curves in the dark and under white light illumination MIS PD_1 (a-b) and MIS PD_2 (c-d). A clear strong increase in photocurrent is observed in presence of Ge NCs.

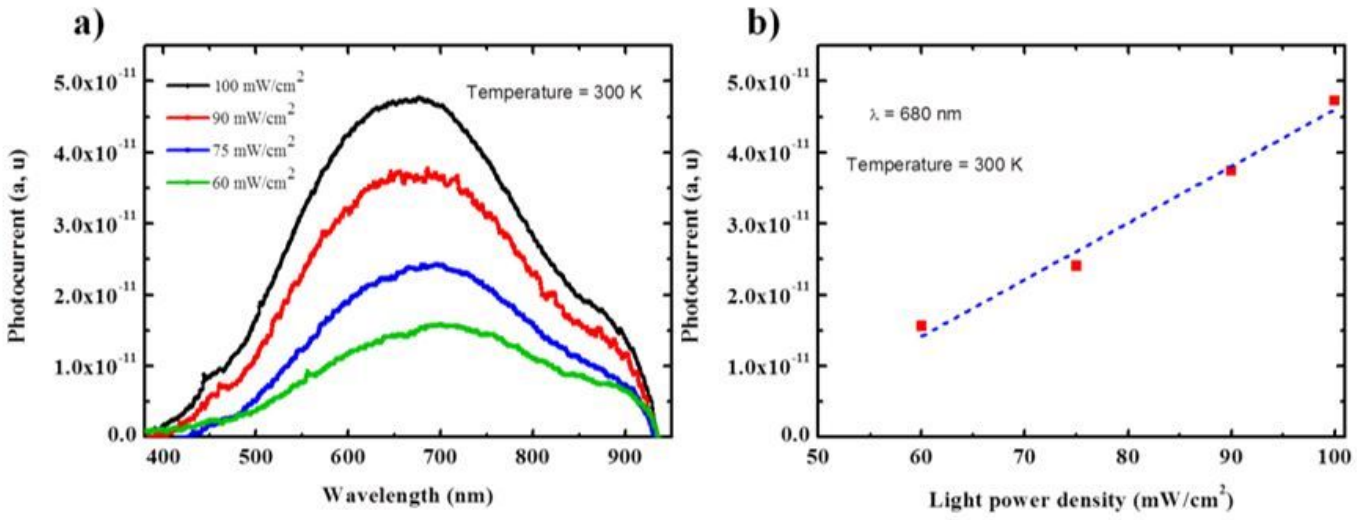

Figure 10

Photocurrent spectra obtained on MIS PD_2 (a). Influence of the 680 nm light power density on the photocurrent intensity of MIS PD_2(b).